



Nanoscale

Formation of Hydrocarbons and Carbon Oxides in MXene Reactions with Water under Varying Oxidative Conditions

Journal:	<i>Nanoscale</i>
Manuscript ID	NR-ART-11-2024-004937.R1
Article Type:	Paper
Date Submitted by the Author:	17-Feb-2025
Complete List of Authors:	Huang, Shuohan; Donghua University Xiang, Guanglei; Donghua University Mochalin, Vadym; Missouri University of Science & Technology, Department of Chemistry; Missouri University of Science & Technology, Department of Materials Science & Engineering

SCHOLARONE™
Manuscripts

Formation of Hydrocarbons and Carbon Oxides in MXene Reactions with Water under Varying Oxidative Conditions

Shuohan Huang^{†,*}, Guanglei Xiang[†], Vadym N. Mochalin^{‡,§,*}

[†]State Key Laboratory of Advanced Fiber Materials, College of Materials Science and Engineering, Donghua University, Shanghai 201620, China

[‡]Department of Chemistry, Missouri University of Science & Technology, Rolla, MO 65409, USA

[§]Department of Materials Science & Engineering, Missouri University of Science & Technology, Rolla, MO 65409, USA

*Corresponding Author: huangs@dhu.edu.cn, mochalinv@mst.edu

ORCID:

Vadym N. Mochalin: 0000-0001-7403-1043

Abstract

Titanium carbide/carbonitride MXenes have garnered significant attention due to their remarkable properties, versatile solution processability, and a broad range of potential applications. However, when exposed to environment, MXenes are susceptible to degradation, which ultimately leads to the formation of metal oxides, a process that may be either adversary or beneficial, depending on the application of a MXene and our knowledge about the underlying mechanisms. Therefore, it is utterly important to understand the reactivity of MXenes in different environments and conditions. Although researchers have made efforts to understand MXene degradation in air and water, our knowledge of the involved processes and even products of degradation remains incomplete. Here, we study the degradation of MXenes (Ti_2CT_x , $\text{Ti}_3\text{C}_2\text{T}_x$, and Ti_3CNT_x) under various oxidative conditions, in presence of hydrogen peroxide, oxygen, ambient air, and argon. Gaseous products of MXene degradation in aqueous environment were examined using gas chromatography (GC) equipped with a thermal conductivity detector (TCD) and a flame ionization detector (FID) working in series. In addition to methane and carbon dioxide, gaseous products including higher hydrocarbons, were identified and analyzed. This research further deepens our understanding of the fundamental chemistry of MXenes.

Introduction

The two-dimensional (2D) transition metal carbides and nitrides, known as MXenes, exhibit a very broad range of compositions compared to other 2D materials.¹ MXenes have the general formula $M_{n+1}X_nT_x$ ($n=1-4$), where M represents an early transition metal, X can be carbon, nitrogen, or oxygen, and T denotes surface terminations such as -OH, -F, and -O-. Over the past decade following their discovery, MXenes have demonstrated exceptional combination of physical and chemical properties, leading to a broad spectrum of potential applications including electromagnetic interference (EMI) shielding^{2, 3}, terahertz spectroscopy and communications⁴, wear reduction and lubrication^{5, 6}, energy storage⁷⁻⁹, molecular/ionic sieving^{10, 11}, sensors¹²⁻¹⁴, composites^{15, 16}, and many others¹⁷⁻¹⁹. However, since their discovery, MXenes have been known to be unstable, particularly in aqueous colloidal solutions, spontaneously transforming into the corresponding metal oxides over time, a process which usually results in loss of their functional properties²⁰, but also provides opportunities to make new materials^{13, 21-23}.

Initial reports have been focused on studying and preventing oxidation as the main mechanism of MXene degradation, and only after the initial discovery of MXene hydrolysis²⁴, an increasing attention has been directed toward understanding the chemical interactions between MXenes and water.^{20, 25, 26} In our own subsequent work, analysis of the gaseous products was established as sensitive and unambiguous technique to detect and monitor MXene degradation²⁷, revealing that carbon and nitrogen in MXenes predominantly form CH_4 and NH_3 , respectively. These experimental discoveries sparked interest of theorists in using quantum chemical modeling to understand the underlying processes. Wu *et al.*²⁸ investigated the interaction between water molecules and the basal plane of $Ti_3C_2O_2$ MXene using *ab initio* molecular dynamics (AIMD) simulations at room temperature (RT). Their findings revealed that the H_2O attack begins with the attachment (chemisorption) of a water molecule onto a Ti atom. This is followed by breaking Ti-C bonds and deprotonation of the water molecule, resulting in the formation of Ti-OH on the $Ti_3C_2O_2$ surface and elimination of an H_3O^+ into the aqueous phase.

Both chemical composition and surface functionalization significantly influence MXene stability. More recently, Song *et al.*²⁹ used AIMD to investigate the interaction between water and defected $Ti_3C_2O_2$ MXene at RT. Their findings reveal that water molecules occupy the O vacancies and dissociate into OH groups and hydronium ions. The hydroxyl groups increase the negative charge

on the MXene surface, which repels water O atoms, hindering their attachment to the Ti sites, thereby reducing the likelihood of further reactions. Additionally, they observed that a high concentration of $-F$ groups on the MXene surface could prevent its degradation. Nesterova et al.³⁰ utilized enhanced sampling AIMD to study the role of terminating groups in chemical stability of $Ti_3C_2T_x$ MXene during its contact with water. Their findings showed that the reactivity of Ti towards water depends on local coordination of Ti sites and the chemical composition of the MXene surface.

Despite these theoretical advancements, AIMD simulations are limited to extremely short time scales, typically picoseconds, meaning they can only capture the very first steps of MXene-water reactions. However, given that MXene degradation is likely a multistep process involving concurrent hydrolysis and oxidation reactions, ionic equilibria and polycondensations leading to transition metal oxides, the theoretical approaches alone cannot fully resolve the reaction mechanisms. This highlights the need for experimental studies to investigate the long-term evolution of MXenes in various environmental conditions. Experimental data not only provide direct evidence of reaction products but also serve as critical input for refining computational models, ultimately improving our understanding of MXene reactivity.

Studies of the reactions of metal carbides with water have a long history, with metal carbides traditionally been divided into two main classes: those that readily react with water or dilute acids, and those that do not.^{31, 32} The carbides decomposable by water or aqueous mineral acids can be further subdivided into three groups: a) forming methane during hydrolysis, like Fe_3C , Be_3C , and Al_4C_3 ; b) forming acetylene upon hydrolysis, like the carbides of the alkali, alkaline earth, and rare earth metals, where $C\equiv C$ linkages exist in the crystal lattice (e.g., CaC_2); and c) forming propyne on hydrolysis, like Mg_2C_3 , because of $C-C\equiv C$ linkages present in its lattice.³² Bulk TiC does not belong to any of these groups, it is inert towards water and is therefore traditionally classified, along with almost all other transition metal carbides, as non-reacting. This classification, although valid for bulk carbides, is being challenged when applied at the nanoscale to 2D forms of transition metal carbides, as we now know that titanium carbide MXenes spontaneously react with water (hydrolysis) in ambient conditions (temperature, pH, oxidizing strength), forming hydrocarbons and carbon oxides, thus showing completely different chemical properties compared to bulk TiC in the key reaction used for classification of carbides, *i.e.*, their hydrolysis.

In view of the above, careful identification of gaseous products of MXene hydrolysis and oxidation is important not only for better understanding of MXene chemistry and ways to improve performance in applications, it also may help us to clarify chemical properties and classification of metal carbides broadly defined. Our initial studies hypothesized about evolution of CO, CO₂, CH₄, and H₂ during MXene hydrolysis, and experimentally confirmed the formation of CO₂ and CH₄.^{24, 27, 33} Later, Doo et al.³⁴ have detected the signals of CH₄, CO, CO₂, and HF during the degradation of Ti₃C₂T_x MXene in water using gas chromatography coupled with time-of-flight mass spectrometry. These results establish a firm basis for the idea that tracing the carbon containing products of MXene hydrolysis can provide valuable information about the fundamental mechanisms of MXene reactivity. To emphasize this idea, we mention parallels with a large body of research on products of bulk carbide hydrolysis. Initial studies of hydrolysis of Mn₃C carbide by Moissan revealed only CH₄ and H₂ as gaseous products, but later studies demonstrated that treatment of manganese carbide samples with hydrochloric acid solutions liberates only part of the carbide's carbon as volatile hydrocarbons, with free carbon and liquid hydrocarbons also being formed in the reaction.³⁵ It is not unlikely that MXene hydrolysis, in addition to already reported CH₄ and CO₂, may yield other products, albeit in smaller quantities. Moreover, the specific ratio of concentrations of different carbon containing products may depend on the nature of 2D carbide, properties of the environment, and conditions of the hydrolytic degradation, for example oxidation strength and acidity of the environment, temperature, *etc.*

In this study, we investigated the volatile carbonaceous degradation products of 3 different titanium MXenes (Ti₂CT_x, Ti₃CNT_x, and Ti₃C₂T_x) exposed to various oxidation environments (aqueous H₂O₂, O₂, air, and Ar) using gas chromatography with a thermal conductivity detector (TCD) and a flame ionization detector (FID) working in series. The GC analysis of these products detected higher hydrocarbons in addition to methane, providing further important insights into the fundamental chemistry of 2D transition metal carbides and carbonitrides (MXenes).

Methods

Synthesis of MAX Phases and MXenes

Ti₂AlC was synthesized by mixing TiC (2 μm size powder, 99.5%, Alfa Aesar), Ti (-325 mesh, 99.5%, Alfa Aesar), and Al (-325 mesh, 99.5%, Alfa Aesar) powders in a molar ratio of 0.85:1.15:1.05. To prevent the formation of transition metal binary carbides, the initial

concentration of Al was adjusted to be slightly higher than the stoichiometric amount.³⁶ The mixture of dry powders was mechanically blended for 12 hours at RT, then heated at 10 °C/min to 1400°C and held at this temperature for 4 hours under Ar flow. Ti_3AlC_2 was synthesized by mixing Ti, Al, and graphite (-325 mesh, 99%, Alfa Aesar) powders in a molar ratio of 3:1.1:1.88. This mixture was also blended for 12 hours and then heated at 10 °C/min to 1550°C and held for 2 hours under Ar flow. Ti_3AlCN was synthesized by mixing Ti, AlN (10 µm size powder, 98%, Sigma-Aldrich), and graphite powders in a molar ratio of 3:1.2:1. The mixture was blended for 12 hours at RT, heated at 10 °C/min to 1550°C, and held at this temperature for 2 hours under Ar flow. The resulting MAX phase ceramic samples were manually crushed using a mortar and pestle.

The synthesis of Ti_2CT_x and $Ti_3C_2T_x$ MXenes followed previously described methods.^{24, 33} The as-synthesized MAX phase powder (Ti_2AlC or Ti_3AlC_2 , 0.3 g, 325 mesh, particle size < 38 µm) was gradually added to an etchant solution prepared by dissolving 0.6 g of LiF (97%, Alfa Aesar) in 6 ml of 9 M HCl (36 wt%, Alfa Aesar) in a loosely capped plastic 50 mL centrifuge tube. The mixture was stirred for 36 hours at 35°C. For the synthesis of Ti_3CNT_x MXene from Ti_3AlCN MAX phase, 0.3 g of Ti_3AlCN powder (325 mesh, particle size < 38 µm) was slowly added to an etchant solution prepared by dissolving 0.8 g of LiF in 10 ml of 9 M HCl in a 50 mL plastic centrifuge tube. The mixture was stirred for 18 hours at 40°C. After etching, the mixtures were washed several times by repeated centrifugation and addition of fresh portions of deionized water until the pH of the supernatant reached approximately 6. Aqueous colloidal solutions of MXenes were obtained by mild ultrasonication at RT for 30 minutes in an ultrasonic bath (Bransonic M2800H) followed by centrifugation for 1 hour at 3500 rpm (Thermo Fisher Scientific Sorvall ST8 Centrifuge). The concentration of the freshly prepared MXene colloidal solutions was approximately 5 mg/mL.

Characterization of MAX phases and MXenes

X-Ray diffraction (XRD) patterns of Ti_3AlC_2 , Ti_3AlCN , and Ti_2AlC MAX phases, as well as $Ti_3C_2T_x$, Ti_3CNT_x , and Ti_2CT_x MXenes were obtained using a Bruker D8 Discover X-ray diffractometer (Diffrac Commander) with Cu K_α radiation ($U = 40$ kV and $I = 40$ mA). The measurements were recorded over a 2θ range from 5° to 85°.

UV–vis spectra of MXene colloidal solutions were measured in a quartz cuvette (1 cm path length) using a PerkinElmer Lambda 35 UV–vis spectrometer, covering a wavelength range of 400–850 nm.

Raman spectra of the MXenes were collected using a Renishaw InVia Raman microscope equipped with a 532 nm laser. Spectra were obtained with a 50× objective and a 1200 lines/mm grating, with an exposure time of 30 s, 1% laser power, and 10 accumulations.

Degradation of MXene samples under different environmental conditions

Four 6 mL aliquots of each MXene solution were transferred into separate 10 mL headspace vials. To the first vial, 100 μL of 30% H_2O_2 (Certified ACS, Thermo Fisher Scientific) was added. The remaining three vials were purged either with O_2 gas (UN1072 UHP, Airgas, 99.994%), ambient compressed air (laboratory-grade, moisture and CO_2 -free, filtered) or Ar gas (UN1006 UHP300, Airgas, 99.999%), correspondingly, by bubbling the gas through the solution for 10 minutes (Figure S1). After purging, the vials were sealed, placed upside down to prevent gas escape through the cap, and stored at room temperature for approximately 1 day for Ti_2CT_x MXene and approximately 5 days for Ti_3CNT_x and $\text{Ti}_3\text{C}_2\text{T}_x$ MXenes, before the aliquots of the gas phase were collected for analysis. For each environmental condition, the experiment was performed at least three times to ensure reproducibility of results. The variability of gas composition measurements was within an acceptable range, with standard deviations provided in the supplementary information (Table S1).

Analysis of gases formed during MXene degradation

Gas samples collected from the MXene samples in water under different atmospheres were analyzed using a Thermo Scientific Trace-1300 gas chromatograph. The instrument was equipped with a fused silica capillary column (Carboxen 1006 PLOT, 30 m length, 0.53 mm diameter, 30 μm thickness) coupled in series with TCD and FID detectors. Helium was used as both carrier and reference gas with flow rates of 4 and 4.3 mL/min, respectively. The parameters for the GC analysis were set as follows. For the first detector in series (TCD) the reference gas flow rate was 4.3 mL/min, the purge flow rate was maintained at 4 mL/min, and the TCD filament temperature

was set to 280°C. For the FID the hydrogen gas, makeup gas (N₂), and air flow rates were 35, 40, and 350 mL/min, respectively, the detector temperature was 250°C. The column temperature was held at 50°C for 4 minutes, then ramped up to 100°C at a rate of 20 °C/min and held for 20 minutes. For each measurement, 0.1 mL of gas was manually injected into GC injector using a 1 mL gastight syringe (Hamilton).

Computational modeling of MXenes and bulk carbides

Atomistic models of monolayer Ti₂C(OH)₂, Ti₃C₂(OH)₂, Ti₃CN(OH)₂, as well as bulk CaC₂ were built and fully optimized using Density Functional Theory (DFT) implemented in CASTEP.³⁷ Full geometry optimization with cell optimization was performed with GGA PBE functional using ultrasoft pseudopotentials with Koelling-Hammon relativistic treatment with plane-wave energy cut-off 380 eV, 3x3x1 *k* points on a Monkhorst-Pack grid, and SCF tolerance 5×10^{-7} eV/atom. Geometry was converged within 5×10^{-6} eV/atom energy, 0.01 eV/Å force, 0.02 GPa stress, and 5×10^{-4} Å displacement. The parameters of the DFT optimized models are provided in Figure S2. These models were used to calculate the carbon-carbon pair distribution functions.

Results and Discussion

Fabrication of MXene dispersions involves etching of aluminum from MAX phases, followed by delamination of multilayer MXenes in aqueous solutions. XRD analysis of Ti₃AlC₂, Ti₃AlCN, and Ti₂AlC MAX phases, along with their corresponding MXenes, confirms good quality of our MAX phases^{2, 24} and successful formation of MXenes, as evidenced by the shift of the (002) peak (Figure 1a-c). UV-vis spectra display characteristic plasmon resonance peaks at ~ 758, 655, and 501 nm for Ti₃C₂T_x, Ti₃CNT_x, and Ti₂CT_x dispersions, respectively (Figure 1d-f)³⁸. Raman spectra of the MXenes (Figure 1g-i), obtained after drying from freshly prepared colloidal solutions, show the expected vibration modes of MXenes, with patterns consistent with reported literature for Ti₃C₂T_x, Ti₃CNT_x, and Ti₂CT_x MXenes^{24, 39}. The full-range Raman spectra in Figure S3 show that the fresh MXenes do not exhibit any significant signals corresponding to sp² or amorphous carbon. Overall, the results of XRD, UV-vis, and Raman characterization confirm the successful synthesis of

MXenes. Furthermore, the morphology of the tested samples was examined using AFM to show all MXene samples were in similar size range and had similar surface morphology (Figure S4).

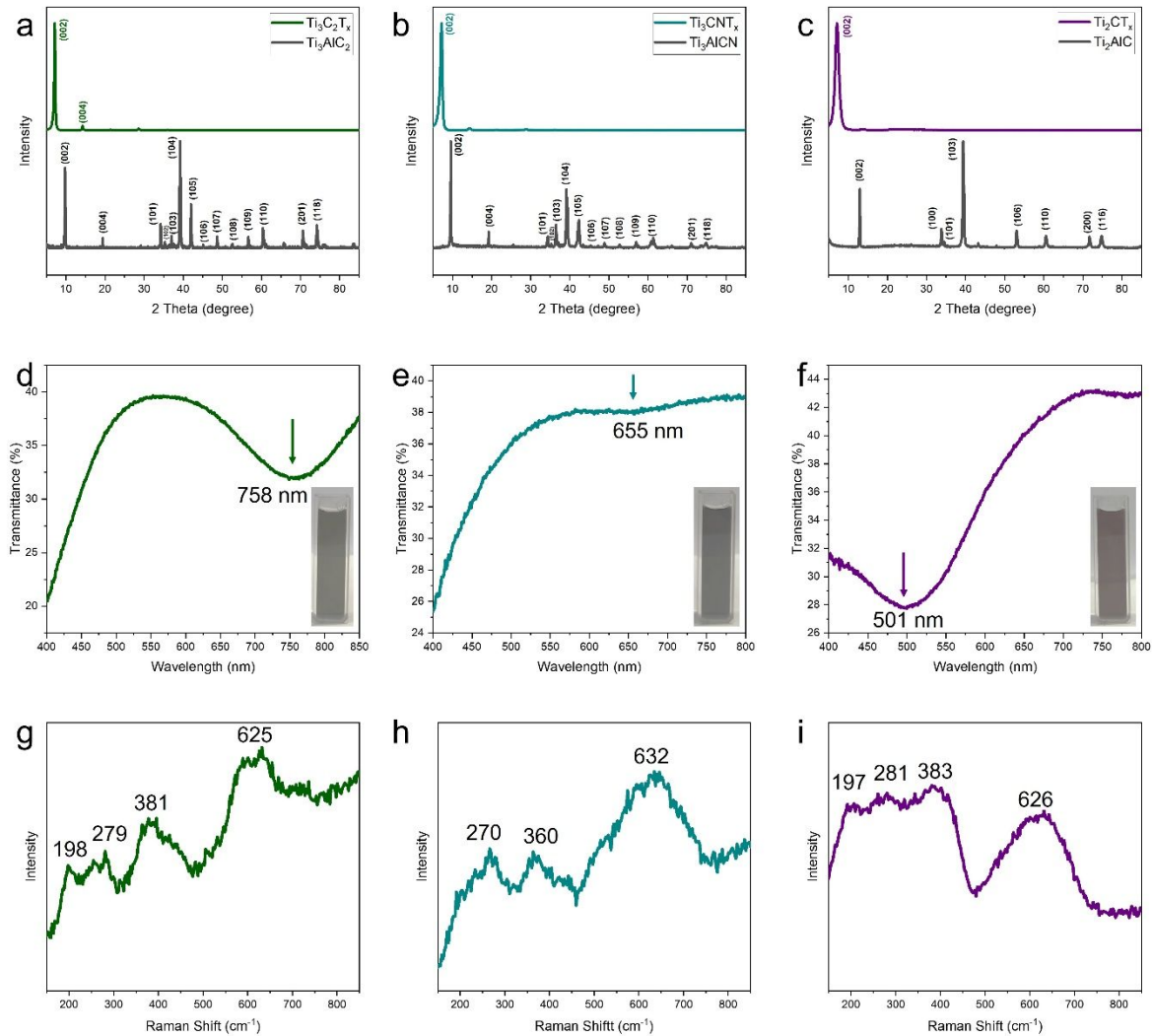


Figure 1. (a-c) XRD patterns of Ti_3AlC_2 , Ti_3AlCN , and Ti_2AlC MAX phases and their corresponding MXenes. (d-f) UV-vis spectra and (g-i) Raman spectra of $Ti_3C_2T_x$, Ti_3CNT_x , and Ti_2CT_x MXenes, respectively.

Gas chromatography results (Figure 2) show composition of the gaseous products from hydrolysis of $Ti_3C_2T_x$ MXene in presence of H_2O_2 . Comparing the retention time of the detected compounds with the corresponding reference gases, we see signals corresponding to CO , CH_4 , and CO_2 with TCD, while the FID detected CO , CH_4 , C_2H_2 (acetylene), C_2H_4 (ethylene), and C_2H_6 (ethane), identified by coincidence of the retention time of the corresponding peaks with the retention time of the corresponding reference gases in same conditions. FID is much more sensitive to

hydrocarbons than TCD, therefore it is not unusual that smaller concentrations of hydrocarbons can be seen with FID while going undetected with TCD. The green-colored area in the bottom panel, which is a zoom-in view of the corresponding narrow area of the FID signal labeled in the middle panel, highlights the peaks of the three mentioned C₂ hydrocarbons and a CO peak. We note that this is the first time when in addition to the previously detected gaseous products (CO, CO₂, and CH₄), C₂ hydrocarbons were detected among the degradation products of MXenes.

Among metal carbides that react with water, LiC₂, CaC₂, SrC₂, and BaC₂ produce pure C₂H₂; Al₄C₃ and Be₂C produce pure CH₄; Mn₃C forms a mixture of H₂ and CH₄; and carbides such as CeC, LaC, YC₂, and ThC₂ react with cold water forming a complex gas mixture containing H₂, C₂H₂, C₂H₄, and CH₄.³¹ Based on the experimental results, titanium carbide MXenes exhibit properties similar to the above listed reactive metal carbides, rather than to their non-reacting bulk “cousin” TiC.

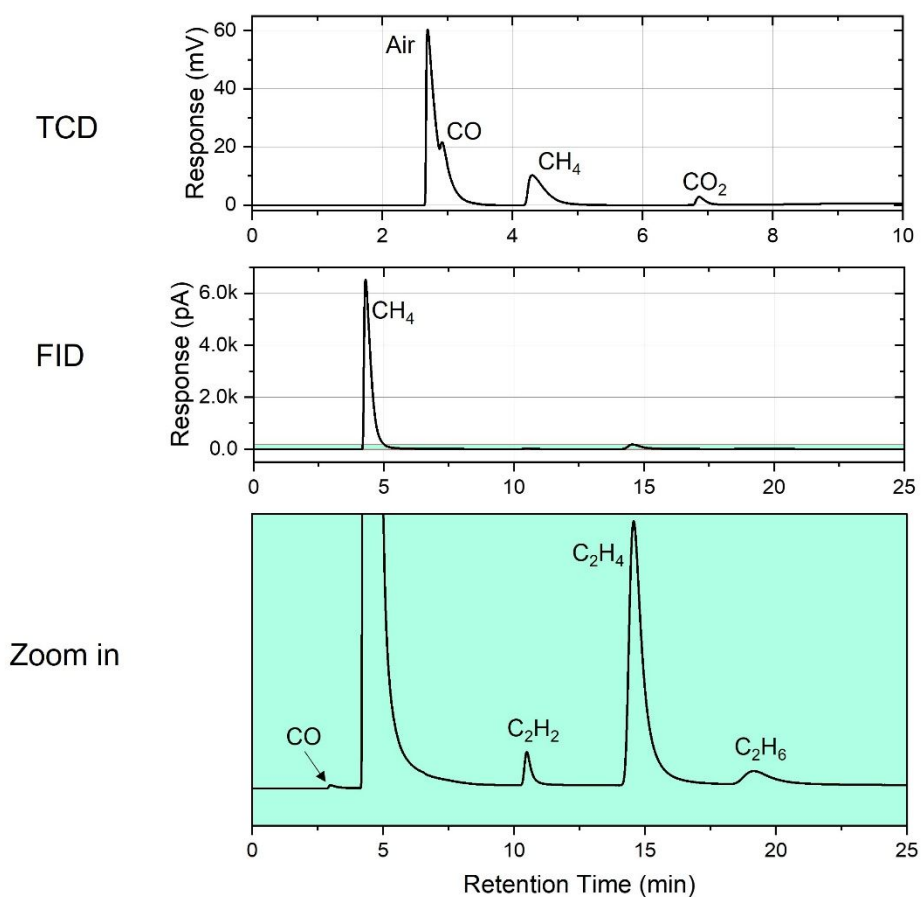


Figure 2. Gas chromatographic analysis of gaseous products collected from hydrolysis of Ti₃C₂T_x MXene in presence of H₂O₂.

In the literature on bulk carbide hydrolysis, the formation of CH_4 is typically explained by the presence of methylene ($=\text{CH}_2$) radicals, which are primary products that undergo hydrogenation and/or polymerization to methane or hydrocarbons with more carbon atoms.³² For example, C_2H_6 is usually discussed as formed through the dimerization of $\text{CH}_3\cdot$ radicals, which are present among hydrolysis products in small amounts. C_2H_2 is usually associated with preexisting $\text{C}\equiv\text{C}$ linkages, and C_2H_4 with $\text{C}=\text{C}$ linkages in the crystalline structure of carbides. However, as shown by radial distribution function analysis (Figure 3), distances between any pair of carbon atoms in the MXene structure greatly exceed C-C, C=C or $\text{C}\equiv\text{C}$ bond length (fully OH terminated models were considered, but changing surface terminations from OH to O, F, or a mix thereof does not change this conclusion). The shortest C-C distances measured with the optimized models are 3.089 Å for $\text{Ti}_3\text{C}_2(\text{OH})_2$, 3.081 Å for $\text{Ti}_2\text{C}(\text{OH})_2$, and 3.073 - 3.093 Å for $\text{Ti}_3\text{CN}(\text{OH})_2$ in contrast to 1.253 Å for CaC_2 . As expected, $\text{Ti}_3\text{CN}(\text{OH})_2$ shows more disorder manifested by slightly broader peaks in its C-C radial distribution function (Figure 3b), therefore we list a range of shortest distances for this MXene.

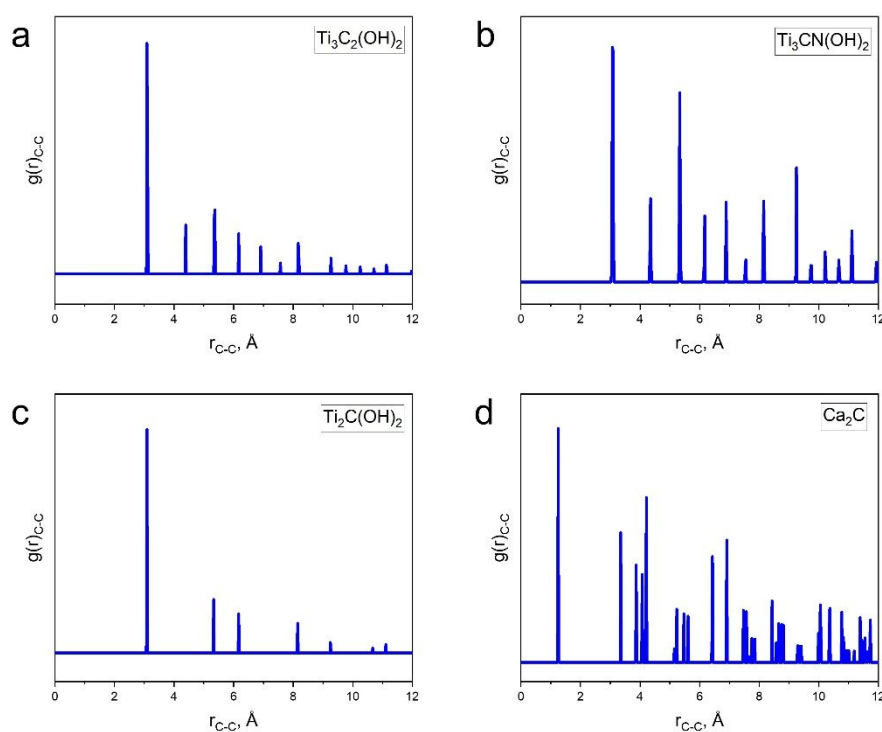


Figure 3. C-C pair distribution functions calculated from atomistic models of (a) $\text{Ti}_3\text{C}_2(\text{OH})_2$, (b) $\text{Ti}_3\text{CN}(\text{OH})_2$, (c) $\text{Ti}_2\text{C}(\text{OH})_2$ MXenes and (d) bulk CaC_2 , which were optimized with Density Functional Theory.

Because there are no existing carbon-carbon linkages in crystalline structure of these MXenes, the most plausible way to form C2 or higher hydrocarbons during MXene hydrolysis is through secondary post-hydrolytic reactions, *e.g.*, radical recombination, which is consistent with the low concentration of these larger molecules that we detected. Their low concentration explains why they were not detected before. Similar radical processes may be involved in the formation of free carbon during oxidative MXene degradation, as reported in some studies.⁴⁰⁻⁴² However, no solid carbon signals were detected in our experiments after the complete degradation of MXenes in water, leading to conclusion that all MXene carbon atoms probably end up in molecular species.
27, 43

The formation of CO in hydrolysis of metal carbides is rarely reported. For instance, only 0.22 % of CO was detected when Mn₃C was hydrolyzed by water at 20°C.³⁵ CO and CO₂ are likely generated from the direct oxidation of MXene carbon by either H₂O or dissolved O₂. Considering MXene as an ionic crystal, the ionic nature of Ti_xC_y, *i.e.*, $Ti_x^{n+}C_y^{n-}$, suggests that electrons can be transferred from Ti atoms to C atoms within the MXene lattice. In the presence of the oxidizer, *e.g.* O₂, once the C atoms gain electrons from the Ti atoms, they become more prone to reducing water, leading to the formation of carbon oxides.⁴⁴

Having identified main and minor gaseous products, we further investigate their quantitative composition. A commercially available standard mixture of different gases was used to determine the gas composition. According to the manufacturer, this mixture included 1.00 mol. % of C₂H₂, 1.00 mol. % of CO₂, 1.00 mol. % of CO, 1.02 mol. % of C₂H₆, 1.00 mol. % of C₂H₄, and 0.999 mol. % of CH₄ (Scotty48, 48 Liters@300 psig, 21°C, analyzed gases). When no strong oxidizers are present in the aqueous MXene colloidal solution, majority of carbon atoms in Ti₃C₂T_x convert to CH₄. As the oxidation potential of the environment increases, the formation of carbon oxides also increases. As shown in Figure 4a, the addition of H₂O₂ to Ti₃C₂T_x aqueous solution resulted in production of 54.33 mol. % CH₄, 2.21 mol. % of C2 hydrocarbons, and 43.46 mol. % carbon oxides. For samples purged with and kept under O₂ atmosphere, the measurements showed 88.51 mol. % CH₄, 3.94 mol. % C2 hydrocarbons, and 7.54 mol. % carbon oxides (Figure 4b). In ambient air environment, the results were 91.09 mol. % CH₄, 4.45 mol. % C2 hydrocarbons, and 4.45 mol. % carbon oxides (Figure 4c). Ti₃C₂T_x aqueous colloids purged with Ar gas produced 93.44 mol. % of CH₄, 4.42 mol. % of C2 hydrocarbons, and 2.14 mol. % of carbon oxides (Figure 4d). Overall,

as the environment became more reducing, the amount of CH_4 among the gas products increased, the amount of C2 hydrocarbons remained relatively constant and small, while the formation of carbon oxides decreased. This is consistent with hydrolysis becoming more pronounced pathway of MXene degradation compared with oxidation in these conditions. Among the detected C2 hydrocarbons, C_2H_4 was consistently formed in greater quantities than C_2H_6 and C_2H_2 , with their amounts remaining relatively similar. Therefore, the nature and content of hydrolysis products of MXenes in water depend on the oxidation potential of the environment.

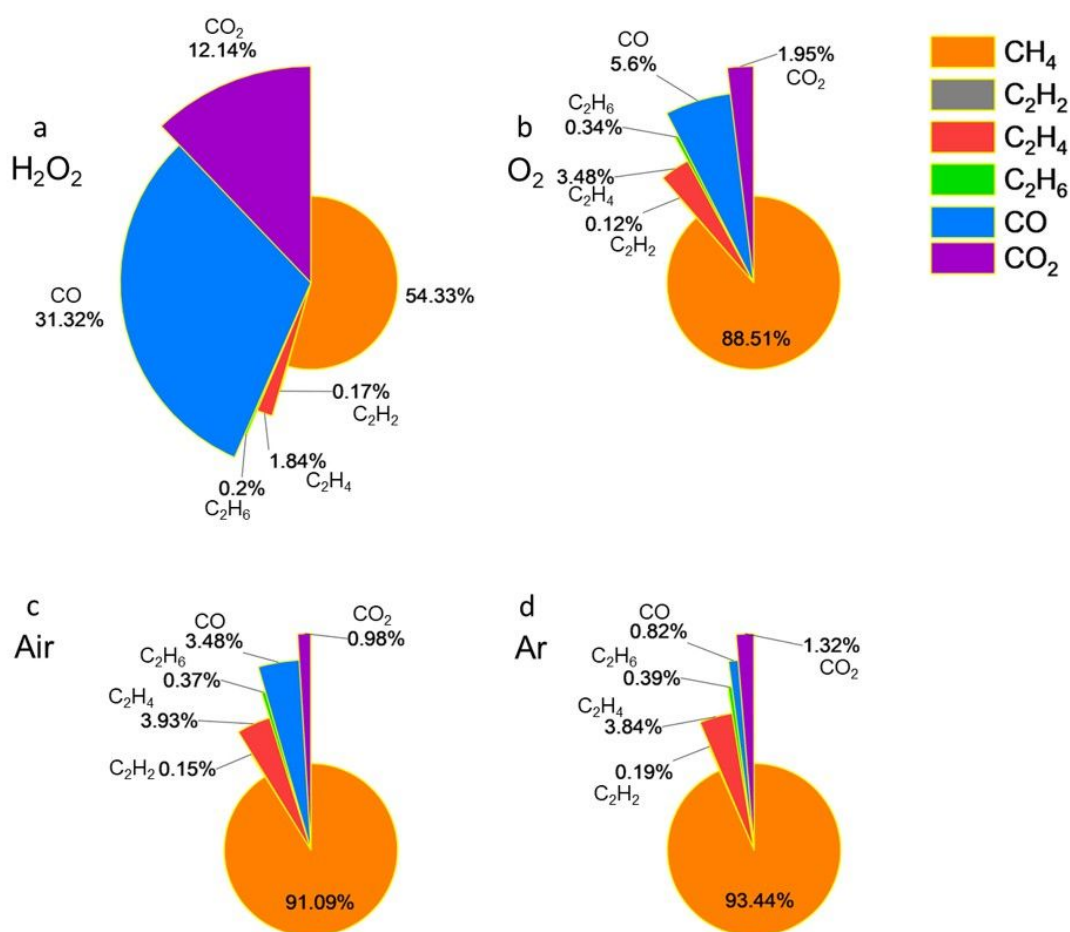


Figure 4. Gaseous product composition of $\text{Ti}_3\text{C}_2\text{T}_x$ aqueous solution under the conditions of (a) H_2O_2 , (b) O_2 , (c) air, and (d) Ar.

As shown in Figure 5a, the addition of H_2O_2 to Ti_3CNT_x aqueous colloidal solution resulted in the production of 33.38 mol. % CH_4 , 2.14 mol. % C2 hydrocarbons, and 64.48 mol. % carbon oxides. Under O_2 atmosphere, the measurements gave 90.84 mol. % CH_4 , 3.37 mol. % C2 hydrocarbons, and 5.79 mol. % carbon oxides (Figure 5b). In an air environment, the results were 95.32 mol. %

CH₄, 2.53 mol. % C₂ hydrocarbons, and 2.15 mol. % carbon oxides (Figure 5c). For Ti₃CNT_x samples purged with Ar gas, the analysis showed 96.75 mol. % CH₄, 2.17 mol. % C₂ hydrocarbons, and 1.08 mol. % CO₂ (well above ~0.04% naturally occurring in ambient air), with no CO detected (Figure 5d).

For Ti₃CNT_x MXene with the addition of H₂O₂, only approximately 33 mol. % of CH₄ was formed, while more than 64 mol. % of gaseous products were carbon oxides. As noted in our prior studies²⁷, compared to Ti₃C₂T_x, random substitution of C atoms with N in Ti₃CNT_x increases reactivity of the material, making it more susceptible to oxidation. Correspondingly, the composition of gases evolved from Ti₃CNT_x under O₂, air, and Ar atmospheres shows a typical ratio of products observed for other studied MXenes above, except that the percentage of CH₄ increased compared to Ti₃C₂T_x in all three environments (O₂, air, and Ar), indicating an even higher reactivity of Ti₃CNT_x in hydrolysis compared to its oxidation, as CH₄ is a product of hydrolysis.

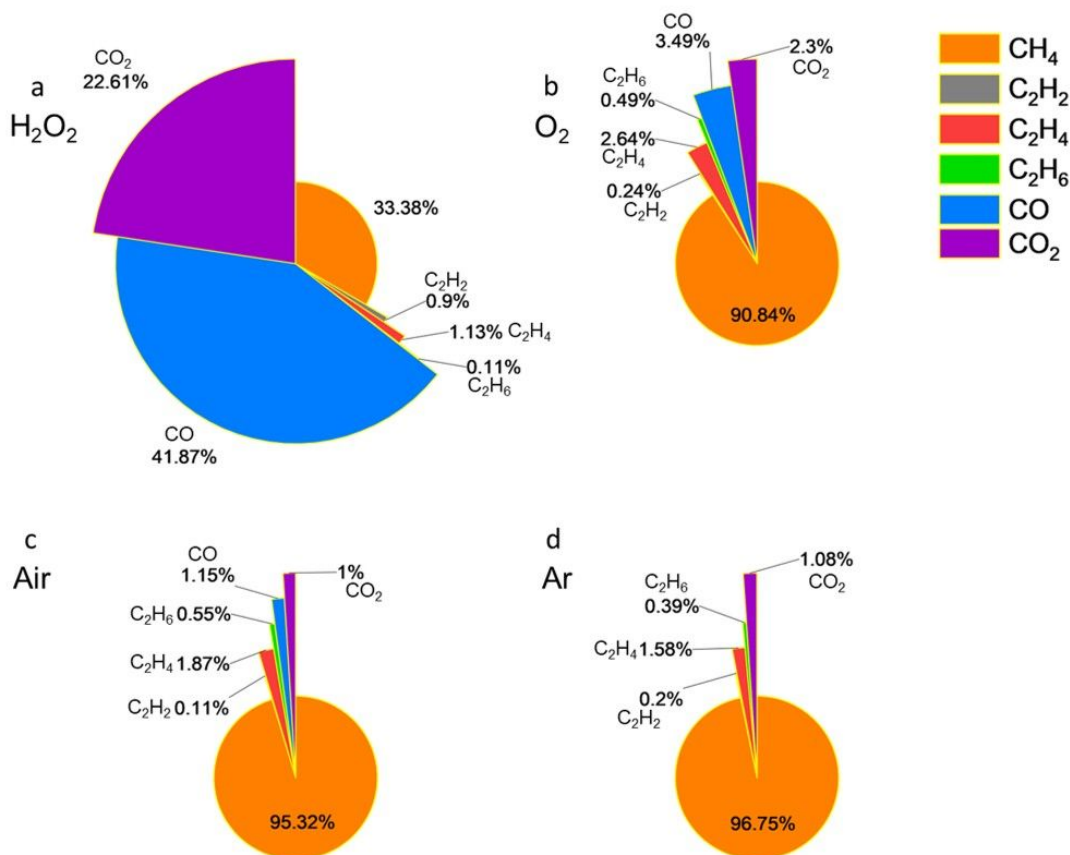


Figure 5. Gaseous product composition of Ti₃CNT_x aqueous solution under the conditions of (a) H₂O₂, (b) O₂, (c) air, and (d) Ar.

The addition of H_2O_2 to the Ti_2CT_x aqueous solution (Figure 6a) resulted in the production of 75.72 mol. % CH_4 , 5.41 mol. % C2 hydrocarbons, and 18.87 mol. % carbon oxides. Under an O_2 atmosphere, 97.86 mol. % CH_4 , 0.58 mol. % C2 hydrocarbons, and 1.56 mol. % CO_2 were formed (with no CO detected, Figure 6b). In an air environment, the results were 98.94 mol. % CH_4 , 0.32 mol. % C2 hydrocarbons, and 0.74 mol. % CO_2 (with no CO detected, Figure 6c). For Ti_2CT_x samples purged with Ar gas, GC analysis showed 99.48 mol. % CH_4 , 0.18 mol. % C2 hydrocarbons, and 0.34 mol. % CO_2 (with no CO detected, Figure 6d). It is worth noting that trace amounts of C_2H_2 , specifically 0.0012 mol.%, 0.0004 mol.%, and 0.0004 mol.%, were still detectable among the degradation products of Ti_2CT_x MXene in contact with O_2 , air, and Ar atmospheres, respectively. But these amounts are insignificant and therefore we do not show them in Figure 6b-d.

For Ti_2CT_x , more CH_4 was produced compared to the other MXenes. This might be explained assuming that higher hydrocarbons are formed in MXene hydrolysis *via* radical recombination processes, and since Ti_2CT_x monolayer contains only one atomic layer of carbon whereas $\text{Ti}_3\text{C}_2\text{T}_x$ and Ti_3CNT_x both contain two, the likelihood of recombination of two radicals formed in the process of stepwise C-Ti bonds breaking during Ti_2CT_x degradation is significantly lower compared to other studied MXenes with a thicker monolayer that provides higher local concentration of C atoms and therefore higher likelihood of radical recombination. When the probability for recombination is low, it is more likely that all carbon atoms will eventually saturate their unsaturated valences by binding hydrogen from water and forming CH_4 , as observed for Ti_2CT_x .

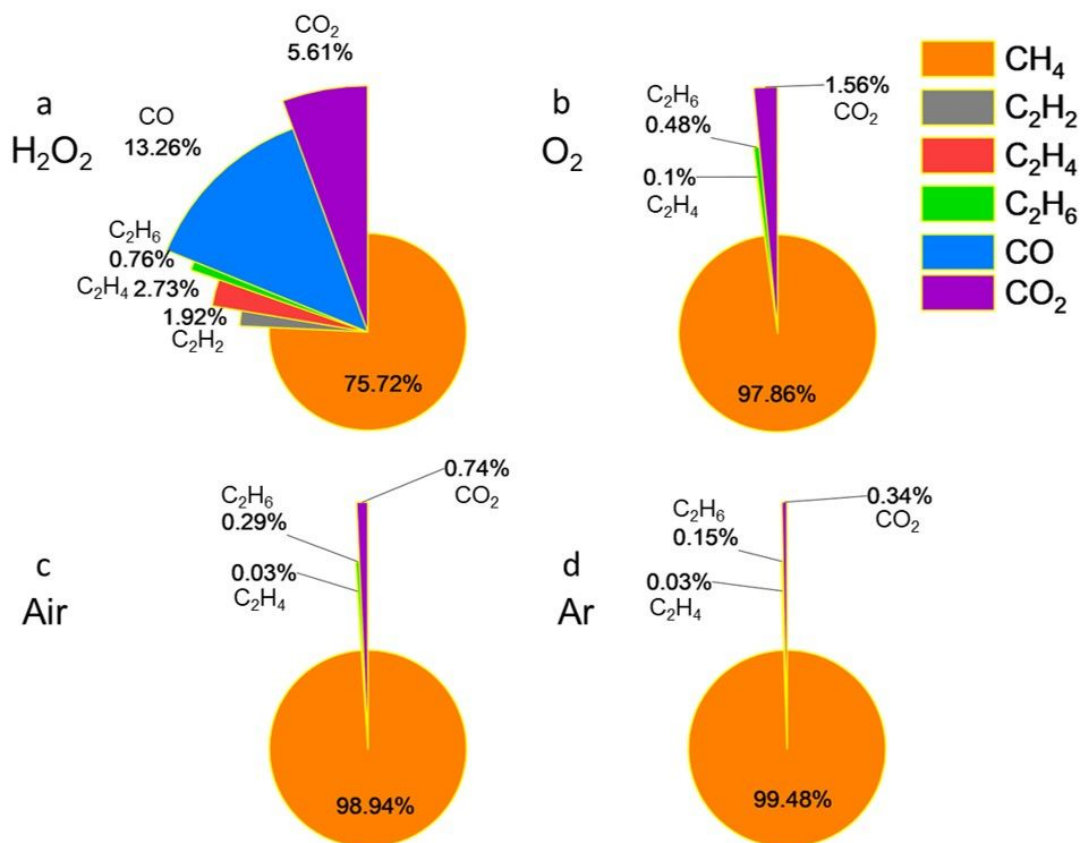


Figure 6. Gaseous product composition of Ti_2CT_x aqueous solution under the conditions of (a) H_2O_2 , (b) O_2 , (c) air, and (d) Ar.

Interestingly, small but measurable quantities of H_2 were detected among degradation products of Ti_2CT_x in aqueous colloids in both air and Ar atmospheres (Figure 7). We never observed H_2 formation with other MXenes and it is not quite clear how it can be formed. One hypothetical source of H_2 might be H^+ , which were evidenced in MXene degradation by drop in pH of solutions over time from freshly made until their complete degradation.²⁷ These protons in solution could in turn originate either from not completely removed HF species or from the reactions of functional groups (at least some of T_x contain hydrogen atoms, *e.g.*, OH), or it could be protons formed by the attack of H_2O on MXene, when OH groups of water are attached to Ti atoms forming $\text{Ti}(\text{OH})_n$ ($n=1-4$) and hydrogen atoms can either attach to C atoms in MXene forming hydrocarbons or, if there is not enough C atoms, will form protons that can be solvated by water and reduced to H_2 later. In the latter case, when there are not enough C atoms for reaction with all H atoms from the attacking water molecules one cannot exclude also recombination of H atoms from water with

direct formation of H_2 . It is not clear at present which of these processes (if any) results in the detected H_2 , but it is noted that we only detect H_2 signal from Ti_2CT_x samples in air and, to a larger extent, in Ar atmospheres, *i.e.*, when the oxidation strength of the environment is relatively low, which agrees with the above mentioned hypotheses.

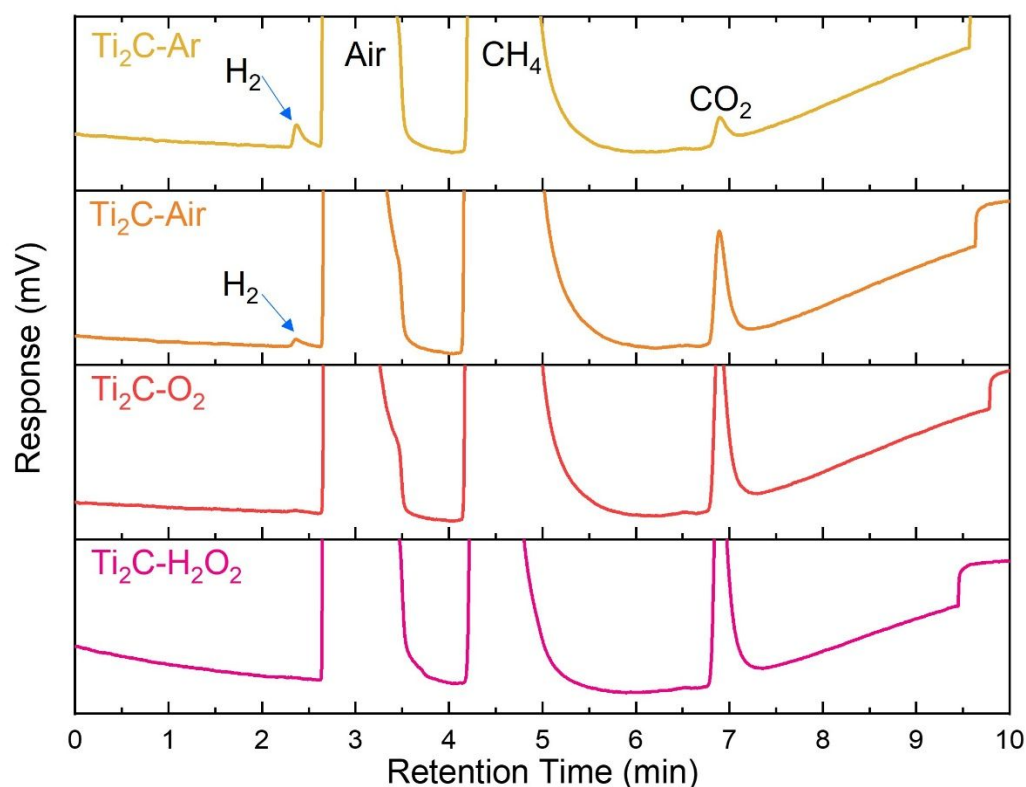


Figure 7. GC-TCD analysis of gaseous products from the hydrolysis of Ti_2CT_x MXene under different environments.

While detection of C2 hydrocarbons among the products of MXene hydrolysis is interesting, we note that even more complex products have been observed in hydrolysis of some of the bulk carbides in the past. For example, bulk uranium carbide, U_2C_3 , when reacted with water yields a significant amount of liquid and solid hydrocarbons in addition to a gaseous mixture containing methane, ethylene, and hydrogen.^{31, 45} Similarly, more complex products, including higher hydrocarbons, may also be anticipated in hydrolysis of MXenes, especially of those MXenes which have not been studied yet and thus, warrant further investigation in future research.

Conclusions

In conclusion, this study explores the degradation behavior of titanium containing MXenes (Ti_2CT_x , $\text{Ti}_3\text{C}_2\text{T}_x$, and Ti_3CNT_x) in water across various oxidation environments, including hydrogen peroxide, oxygen, air, and argon. Gas chromatography analysis revealed the formation of gaseous products such as methane, carbon oxides, and, for the first time, C2 hydrocarbons (ethylene, acetylene, and ethane), broadening our understanding of MXene chemistry. According to our results, methane is the dominant product under reducing conditions, while production of carbon oxides increases in the environments with higher oxidation potential. This research offers insights into the hydrolysis and oxidative degradation mechanisms of MXenes, in comparison to bulk metal carbides, thereby challenging our traditional knowledge of carbide chemistry. We believe that this information will also contribute to a more rational development of various applications of MXenes.

Author contributions

Shuohan Huang – writing – original draft, methodology, data curation, conceptualization, and funding acquisition; Guanglei Xiang – formal analysis, writing – review and editing, and validation; Vadym N. Mochalin – writing – review and editing, conceptualization, supervision, and funding acquisition.

Data availability

The data supporting this article have been included as part of the Supplementary Information.

Conflicts of interest

The authors declare that they have no known competing financial interests or personal relationships that could have appeared to influence the work reported in this paper.

Acknowledgements

This work was supported by National Natural Science Foundation of China (No. 52402102) and Fundamental Research Funds for the Central Universities (2232022D-03). We acknowledge funding support of this research from the National Science Foundation (DMREF-2324156).

References

1. M. Naguib, V. N. Mochalin, M. W. Barsoum and Y. Gogotsi, *Adv. Mater.*, 2014, **26**, 992-1005.
2. A. Iqbal, F. Shahzad, K. Hantanasirisakul, M.-K. Kim, J. Kwon, J. Hong, H. Kim, D. Kim, Y. Gogotsi and C. M. Koo, *Science*, 2020, **369**, 446-450.
3. C. Liu, Y. Ma, Y. Xie, J. Zou, H. Wu, S. Peng, W. Qian, D. He, X. Zhang, B.-W. Li and C.-W. Nan, *ACS Appl. Mater. Interfaces*, 2023, **15**, 4516-4526.
4. G. Li, N. Amer, H. A. Hafez, S. Huang, D. Turchinovich, V. N. Mochalin, F. A. Hegmann and L. V. Titova, *Nano Lett.*, 2020, **20**, 636-643.
5. S. Huang, K. C. Mutyala, A. V. Sumant and V. N. Mochalin, *Mater. Today Adv.*, 2021, **9**, 100133.
6. A. Rosenkranz, M. C. Righi, A. V. Sumant, B. Anasori and V. N. Mochalin, *Adv. Mater.*, 2023, **35**, 2207757.
7. J. Yang, M. Li, S. Fang, Y. Wang, H. He, C. Wang, Z. Zhang, B. Yuan, L. Jiang, R. H. Baughman and Q. Cheng, *Science*, 2024, **383**, 771-777.
8. M. Lai, C. Zhao, D. Wang, R. Gao, P. Cai, L. Sun, Q. He, H. Peng, H. Zhang, F. Xu, C. Hu, K. Liang and C. J. Zhang, *ACS Appl. Mater. Interfaces*, 2024, **16**, 55555-55568.
9. W. Zhang, C. Zeng, M. Zhang, C. Zhao, D. Chao, G. Zhou and C. Zhang, *Angew. Chem. Int. Ed*, 2025, **64**, e202413728.
10. X. Zhu, M. Lou, J. Chen, X. Fang, S. Huang and F. Li, *Appl. Surf. Sci.*, 2023, **625**, 157194.
11. Y. Li, X. Zhu, Q. Gao, Y. Bai, M. Lou, S. Huang, F. Li and B. Van der Bruggen, *J. Membr. Sci.*, 2024, **712**, 123236.
12. H. Zhang, Y. He, Y. Xia, Y. Chen, Y. Wang, R. Weng, T. Zhang and S. Huang, *Mater. Today Chem.*, 2024, **38**, 102088.
13. S. Chertopalov and V. N. Mochalin, *ACS Nano*, 2018, **12**, 6109-6116.
14. Q. He, C. Zhao, H. Chen, T. Wu, C. Zeng, Y. Chen and C. Zhang, *J. Mater. Chem. A*, 2024, **12**, 25622-25642.
15. L. Bi, W. Perry, R. Wang, R. Lord, T. Hryhorchuk, A. Inman, O. Gogotsi, V. Balitskiy, V. Zahorodna, I. Baginskiy, S. Vorotilo and Y. Gogotsi, *Adv. Funct. Mater.*, 2023, **34**, 2312434.
16. A. Baimenov, C. Daulbayev, S. G. Pouloupoulos and V. N. Mochalin, *Mater. Today*, 2024, **78**, 75-91.
17. S. Abdolhosseinzadeh, R. Schneider, M. Jafarpour, C. Merlet, F. Nüesch, C. Zhang and J. Heier, *Adv. Electron. Mater.*, 2025, **11**, 2400170.
18. T. Guo, D. Zhou, S. Deng, M. Jafarpour, J. Avaro, A. Neels, J. Heier and C. Zhang, *ACS Nano*, 2023, **17**, 3737-3749.
19. T. Guo, D. Zhou, M. Gao, S. Deng, M. Jafarpour, J. Avaro, A. Neels, E. Hack, J. Wang, J. Heier and C. Zhang, *Adv. Funct. Mater.*, 2023, **33**, 2213183.
20. K. P. Marquez, K. M. D. Sisican, R. P. Ibabao, R. A. J. Malenab, M. A. N. Judicpa, L. Henderson, J. Zhang, K. A. S. Usman and J. M. Razal, *Small Sci.*, 2024, **4**, 2400150.
21. P. Ridley, C. Gallano, R. Andris, C. E. Shuck, Y. Gogotsi and E. Pomerantseva, *ACS Appl. Energy Mater.*, 2020, **3**, 10892-10901.
22. M. A. K. Purbayanto, M. Chandel, D. Bury, A. Wójcik, D. Moszczyńska, A. Tabassum, V. N. Mochalin, M. Naguib and A. M. Jastrzębska, *Langmuir*, 2024, **40**, 21547-21558.

23. M. A. K. Purbayanto, D. Bury, M. Chandel, Z. D. Shahrak, V. N. Mochalin, A. Wójcik, D. Moszczyńska, A. Wojciechowska, A. Tabassum, M. Naguib and A. M. Jastrzębska, *ACS Appl. Mater. Interfaces*, 2023, **15**, 44075-44086.
24. S. Huang and V. N. Mochalin, *Inorg. Chem.*, 2019, **58**, 1958-1966.
25. F. Cao, Y. Zhang, H. Wang, K. Khan, A. K. Tareen, W. Qian, H. Zhang and H. Ågren, *Adv. Mater.*, 2022, **34**, 2107554.
26. R. A. Soomro, P. Zhang, B. Fan, Y. Wei and B. Xu, *Nanomicro Lett.*, 2023, **15**, 108.
27. S. Huang and V. N. Mochalin, *ACS Nano*, 2020, **14**, 10251-10257.
28. T. Wu, P. R. C. Kent, Y. Gogotsi and D.-e. Jiang, *Chem. Mater.*, 2022, **34**, 4975-4982.
29. H. Song and D.-e. Jiang, *Nanoscale*, 2023, **15**, 16010-16015.
30. V. Nesterova, V. Korostelev and K. Klyukin, *J. Phys. Chem. Lett.*, 2024, **15**, 3698-3704.
31. G. N. H., *Nature*, 1896, **54**, 357-357.
32. G. L. Putnam and K. A. Kobe, *Chem. Rev.*, 1937, **20**, 131-143.
33. S. Huang, V. Natu, J. Tao, Y. Xia, V. N. Mochalin and M. W. Barsoum, *J. Mater. Chem. A*, 2022, **10**, 22016-22024.
34. S. Doo, A. Chae, D. Kim, T. Oh, T. Y. Ko, S. J. Kim, D.-Y. Koh and C. M. Koo, *ACS Appl. Mater. Interfaces*, 2021, **13**, 22855-22865.
35. W. R. Myers and W. Fishel, *J. Am. Chem. Soc.*, 1945, **67**, 1962-1964.
36. M. N. Abdelmalak, *MXenes: A new family of two-dimensional materials and its application as electrodes for Li-ion batteries*, Drexel University, 2014.
37. S. J. Clark, M. D. Segall, C. J. Pickard, P. J. Hasnip, M. I. J. Probert, K. Refson and M. C. Payne, *Z. fur Krist. - Cryst. Mater.*, 2005, **220**, 567-570.
38. K. Shevchuk, A. Sarycheva and Y. Gogotsi, *MRS Bull.*, 2022, **47**, 545-554.
39. S. Huang and V. N. Mochalin, *Inorg. Chem.*, 2022, **61**, 9877-9887.
40. H. Ghassemi, W. Harlow, O. Mashtalir, M. Beidaghi, M. Lukatskaya, Y. Gogotsi and M. L. Taheri, *J. Mater. Chem. A*, 2014, **2**, 14339-14343.
41. M. Naguib, O. Mashtalir, M. R. Lukatskaya, B. Dyatkin, C. Zhang, V. Presser, Y. Gogotsi and M. W. Barsoum, *Chem. Commun.*, 2014, **50**, 7420-7423.
42. Y. Liu, Z. Shi, T. Liang, D. Zheng, Z. Yang, Z. Wang, J. Zhou and S. Wang, *InfoMat*, 2024, **6**, e12536.
43. B. Ahmed, D. H. Anjum, M. N. Hedhili, Y. Gogotsi and H. N. Alshareef, *Nanoscale*, 2016, **8**, 7580-7587.
44. Y. Hori and T. Mukaibo, *Bull. Chem. Soc. Jpn*, 1968, **41**, 1983-1989.
45. S. El Jamal, M. Johnsson and M. Jonsson, *ACS Omega*, 2021, **6**, 24289-24295.

Data availability

The data supporting this article have been included as part of the Supplementary Information.